Available online at www.sciencedirect.com
SCIENCE DIRECT®
Journal of Solid State Chemistry 174 (2003) 372–380
JOURNAL OF SOLID STATE CHEMISTRY
http://elsevier.com/locate/jssc

The effect of F^--doping and temperature on the structural and textural evolution of mesoporous TiO_2 powders

Jia-Guo Yu,[a,*] Jimmy C Yu,[b] Bei Cheng,[a] S.K. Hark,[c] and Kwansai Iu[c]

[a] *State Key Laboratory of Advanced Technology for Materials Synthesis and Processing, Wuhan University of Technology, Wuhan 430070, China*
[b] *Department of Chemistry and Materials Science and Technology Research Centre, China*
[c] *Department of Physics, The Chinese University of Hong Kong, Shatin, New Territories, Hong Kong, China*

Received 21 January 2003; received in revised form 11 April 2003; accepted 26 April 2003

Abstract

Mesoporous F^--doped TiO_2 powders were prepared by hydrolysis of titanium tetraisopropoxide (TTIP) in a mixed NH_4F–H_2O solution. Effects of F^- ion content and calcination temperatures on the phase composition and porosity of mesoporous titania were investigated by X-ray diffraction (XRD), transmission electron microscopy (TEM), scanning electron microscopy (SEM) and BET surface areas. The results showed the BET surface area (S_{BET}) of the pure and doped powders dried at 100°C ranged from 260 to 310 m^2/g as determined by nitrogen adsorption. With increasing calcination temperatures, the S_{BET} values of the calcined titania powders decreased due to the increase in crystalline size. The pore size distribution was bimodal with fine intra-particle pore and larger inter-particle pore as determined by nitrogen adsorption isotherms. The peak pore diameter of intra-particle pore increases with increasing F^- ion content. At 700°C, all the titania powders exhibit monomodal pore size distributions due to the complete collapse of the intra-particle pores. The crystallization of anatase was obviously enhanced due to F^--doping at 400°C and 500°C. Moreover, with increasing F^- ion concent, F^- ions not only suppressed the formation of brookite phase at low temperature, but also prevented phase transition of anatase to rutile at high temperature.

Keywords: Mesoporous titania powders; F^--doping; Bimodal pore size distribution; Phase composition

1. Introduction

Titania has been studied extensively because of its wide applications in pigments, photocatalysts, catalytic supports, filters, coatings, cosmetics, adsorbents, sensors and photoconductors, etc. [1–6]. In these applications, the control of morphology, particle size, particle size distribution, phase composition, and porosity of the titania powders is an important factor in determining the properties of the final material [6–8]. On a commercial scale, titania powders are typically made in the liquid or gas phase by the sulfate and chloride processes, respectively. The chloride process produces titania particles by oxidation of titanium tetrachloride ($TiCl_4$) vapor in a flame reactor. In the liquid phase, TiO_2 powders are usually prepared by wet precipitation from $TiO(SO_4)$, $Ti(SO_4)_2$ or $TiCl_4$. However, the counter anions of the starting titanium salts may remain in the product and deteriorate the purity of the powders.

Sol–gel route provides a way of making nanoparticle materials by a chemical reaction in solution starting with metal alkoxide as a precursor. The advantages of the sol–gel method include precise control of pore structure, dopant concentration, and chemical purity [9–11]. In this synthesis route hydrolysis and polycondensation reactions take place when TTIP reacts with water. These two reactions form nuclei (2–10 nm in diameter), which develop into primary particles (50–100 nm in diameter). These primary particles aggregate to form secondary particles (300–1000 nm in diameter) during aging [12]. When solvent is removed (solvent evaporation) from the solution, these secondary particles agglomerate to form dried powders (xerogel powders) with large shrinkage.

Many researchers have studied extensively the retardation of phase transformation by doping TiO_2 with a second oxide or metal ions. This can reduce the sintering

*Corresponding author.
E-mail addresses: yujiaguo@public.wh.hb.cn (J.-G. Yu), jimyu@cuhk.edu.hk (J.C. Yu).

0022-4596/03/$ - see front matter © 2003 Elsevier Inc. All rights reserved.
doi:10.1016/S0022-4596(03)00250-0

rates and nucleation sites (in grain boundary or in bulk) or increase the nucleation activation energy [13,14]. Kumar et al. [15] studied the effect of alumina on phase and pore structure of titania membranes. They reported that the anatase to rutile phase transformation temperature of the alumina–titania composite membrane (50 wt% alumina) was 300°C higher than that of pure titania. Yang et al. [16–18] extensively studied the effect of alumina, silica, zirconia, and alumina–silica additives on the titania phase transformation, All these additives showed inhibitory effects on the titania phase transformation, and at the same dopant concentration (dopant/Ti = 0.1), the alumina/silica mixed additive showed the most enhanced retarding effect over other single additives. Vargas et al. [19] investigated the effect of cationic dopants on the phase transformation temperature of titania. They chose a large set of metal dopants from different groups of the periodic table to find the relationship between the anatase to rutile phase transformation temperature and ionic radii. Recently, Kim et al. [14] reported alumina, zirconia and silica doped titania powders retarded the anatase to rutile phase transformation and showed a significantly improved textural stability compared to the pure titania powders. Yanagisama et al. [20] found that the chloride ion can accelerate the nucleation of the anatase under hydrothermal conditions. Yin et al. [21] also reported that the nano-sized anatase and rutile TiO_2 powders were prepared using amorphous phase TiO_2 by hydrothermal processes in the presence of HF and HCl as cooperative catalyst. Very recently, we have reported the effects of PbO- and SiO_2-doping on microstructures and photocatalytic activity of TiO_2 thin film photocatalysts [22,23]. Although the above studies addressed the effect of cationic dopants (or metal oxide doping) on the pore structures and phase stability of titania, little is known about the resulting pore structure and phase stability of anionic doped titania.

Very recently, we have also reported the enhancing effects of F^--doping on photocatalytic activity of nanometer-sized TiO_2 powders prepared by the sol–gel method, and the photocatalytic activity of the obtained F^--doped TiO_2 powders exceeded that of Degussa P25 [24]. However, to the best of our knowledge, effects of F^- ion content and calcination temperatures on the structural and textural evolution of TiO_2 powders prepared by hydrolysis of TTIP have not been reported in the previous literature. In this study, mesoporous nano-sized F^--doped TiO_2 photocatalyst has been prepared by sol-gel method and ultrasonic treatment from pure water. The effects of initial F^- ion content and calcination temperatures on the characteristics of mesoporous titania powders were investigated by X-ray diffraction (XRD), nitrogen adsorption, transmission electron micrograph (TEM) and scanning electron micrograph (SEM).

2. Experimental

2.1. Preparation

All chemicals used in this study were reagent-grade supplied from Aldrich and were used as received. Millipore water was used in all experiments.

Titanium tetraisopropoxide (TTIP) was used as a titanium source. NH_4F as a precursor of the dopant was dissolved in pure water. Then TTIP (0.125 mol) was added dropwise to 100 mL of the H_2O–NH_4F mixed solution under vigorous stirring at room temperature. The atomic ratios of F to Ti, which hereafter was designated as R_F, were 0, 1, 5, 10 and 20 nominal atomic % (at.%). Sol samples obtained by the hydrolysis process were aged in a closed beaker at room temperature for 24 h in order to further hydrolyze the TTIP. After aging, these samples were dried at 100°C for about 12 h in air in order to vaporize water and alcohol in the gels and then ground to fine powders to obtain xerogel samples. The xerogel samples were calcined at temperatures of 400, 500, 600 and 700°C in air for 1 h.

2.2. Characterization

The XRD patterns obtained on a Philips MPD 18801 X-ray diffractometer using Cu$K\alpha$ radiation at a scan rate of 0.05° 2θ S^{-1} were used to determine the identity of any phase present and their crystallite size. The accelerating voltage and the applied current were 35 kV and 20 mA, respectively. The phase content of a sample was calculated from the integrated intensities of anatase (101), rutile (110) and brookite (121) peaks according to literature [25,26]. If a sample contains anatase, rutile and brookite, the mass fraction of anatase (W_A), rutile (W_R) and brookite (W_B) can be calculated from [26]

$$W_A = \frac{K_A A_A}{K_A A_A + A_R + K_B A_B}, \quad (1a)$$

$$W_R = \frac{A_R}{K_A A_A + A_R + K_B A_B}, \quad (1b)$$

$$W_B = \frac{K_B A_B}{K_A A_A + A_R + K_B A_B}, \quad (1c)$$

where A_A, A_R and A_B are the integrated intensity of the anatase (101), rutile (110) and brookite (121) peaks, respectively, W_A, W_R and W_B represent the mass fraction of anatase, rutile and brookite, respectively, and K_A and K_B are two coefficients and their values are 0.886 and 2.721, respectively. With Eq. (1), the phase contents in any TiO_2 samples can be calculated. The average crystallite sizes of anatase, rutile, and brookite were determined according to the Scherrer equation using the fwhm data of each phase after correcting the instrumental broading [25,26].

Normally, the anatase phase of titania is the main product in hydrolytic sol–gel synthesis of nanocrystalline titania. However, brookite is also typically present in synthesis products. Brookite can be detected by the appearance of its (121) peak in powder X-ray diffraction (XRD) patterns at $2\theta = 30.8°$. However, in many previous studies, the existence of this brookite phase was overlooked [27,28]. Even if the intensity of the brookite (121) peak is very low compared to the anatase (101) peak, the amount of brookite may be considerable [26,29].

Crystallite sizes and shapes were observed using transmission electron microscopy (TEM) (JCOL Co., 1200EX, Japan). Particle sizes and shapes were observed using scanning electron microscopy (SEM) (JSM-5610LV, Japan). The Brunauer–Emmett–Teller (BET) surface area (S_{BET}) of the powders was analyzed by nitrogen adsorption in a Micromeritics ASAP 2000 nitrogen adsorption apparatus. For xerogel samples dried at 100°C, the samples were degassed at 100°C prior to actual measurements. However, for the calcined xerogel samples at high temperature (from 400°C to 700°C), the degassed temperature is 180°C. The BET surface area was determined by the multipoint BET method using the adsorption data in the relative pressure (P/P_0) range 0.05–0.25. The desorption isotherm was used to determine the pore size distribution using the Barret, Joyner, and Halender (BJH) method with cylindrical pore size [30].

3. Results and discussion

3.1. Crystal structure

Fig. 1 shows the effects of R_F on phase structures of the TiO_2 xerogel powders prepared from the H_2O–NH_4F mixed solution and dried at 100°C for 8 h [24]. The anatase phase is dominant in the as-prepared TiO_2 xerogel powder from pure water ($R_F = 0$), but there is a small amount of brookite in it. The small peak at $2\theta = 30.7°$ corresponds to the (121) plane of the brookite phase of titania. The presence of this phase causes the slight shift to higher angle of the anatase peak (101), since there is an overlapping between brookite peak (120) and anatase peak (101). Fig. 2 shows the effects of R_F on anatase and brookite phase content of TiO_2 xerogel powders dried at 100°C for 8 h. It can be seen from Fig. 2 that with increasing R_F, the content of anatase phase steadily increases and finally become 100% when $R_F \geqslant 10$. This can be ascribed to the fact that F^- ions enhance the crystallization of anatase phase, and meanwhile suppress the crystallization of brookite phase by adsorbing on to the surfaces of TiO_2 particles [20,21,24].

Figs. 3(a)–(c) show XRD patterns of TiO_2 powders prepared from the H_2O–NH_4F mixed solution with $R_F = 0$ (a), 5 (b) and 10 (c), respectively, and calcined at various temperatures. It can be seen that with increasing calcination temperature (from 100°C to 600°C), the peak intensities of anatase increase and the width of the (101) plane diffraction peak of anatase ($2\theta = 25.4°$) become narrower. When $R_F = 0$, the rutile phase starts to appear at 600°C. TiO_2 powders thus contain three different phases: anatase, brookite snd rutile. At 700°C, rutile is a main phase and brookite disappears. When $R_F = 5$, the rutile phase starts to appear at 700°C. At 700°C, TiO_2 powders contain three different phases: anatase, brookite and rutile; anatase also is a main phase. When $R_F = 10$, the resulting TiO_2 powders contain only anatase phase over the calcination temperature range from 100°C to 700°C. The processes of phase transformation occurring in the above three samples at different temperature are illustrated in Fig. 4.

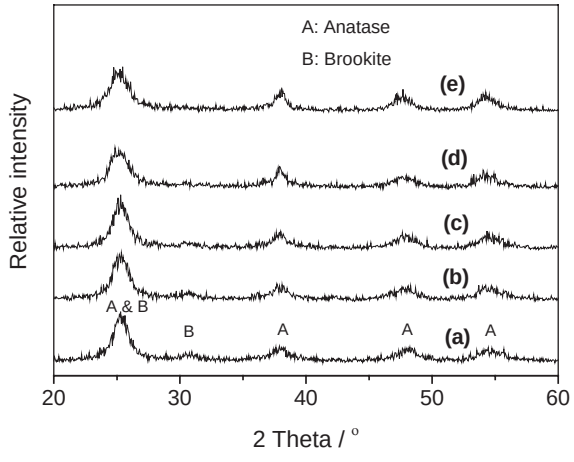

Fig. 1. XRD patterns of the TiO_2 xerogel powders prepared from the H_2O–NH_4F mixed solution with $R_F = 0$ (pure water) (a), 1 (b), 5 (c), 10 (d) and 20(e); and dried at 100°C for 8 h [24].

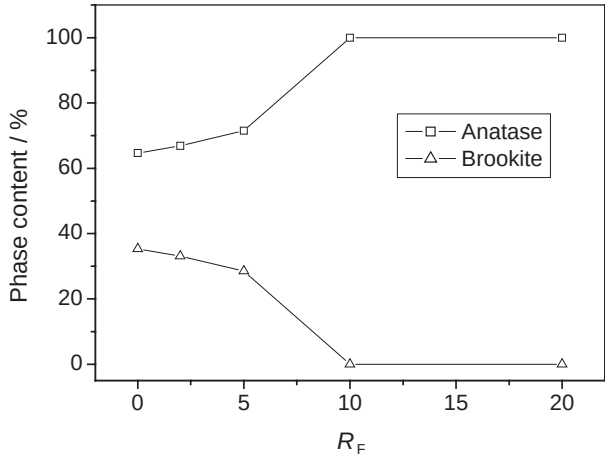

Fig. 2. Effects of R_F on anatase and brookite phase content of TiO_2 xerogel powders dried at 100°C for 8 h.

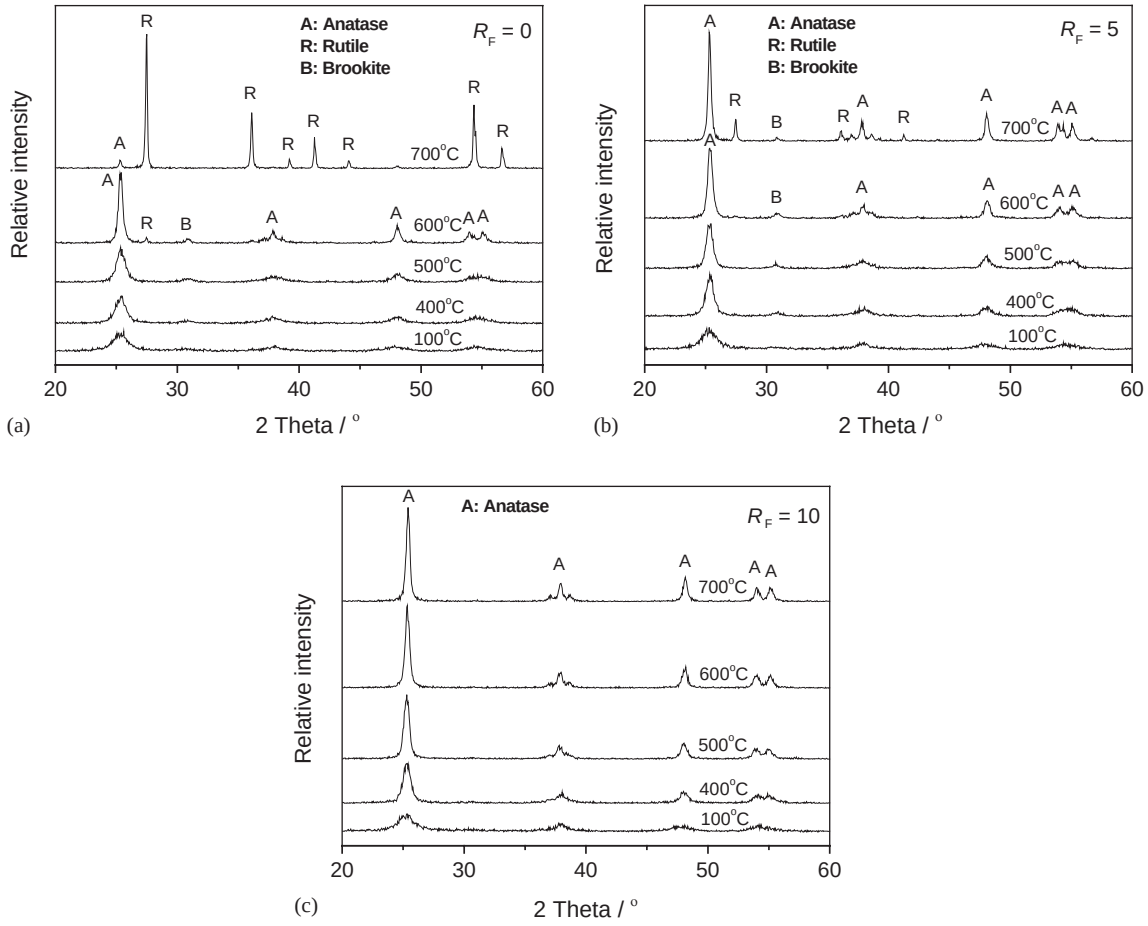

Fig. 3. XRD patterns of TiO_2 powders prepared from the H_2O–NH_4F mixed solution with (a) $R_F = 0$, (b) $R_F = 5$ and (c) $R_F = 10$, and calcined at 100°C, 400°C, 500°C, 600°C and 700°C.

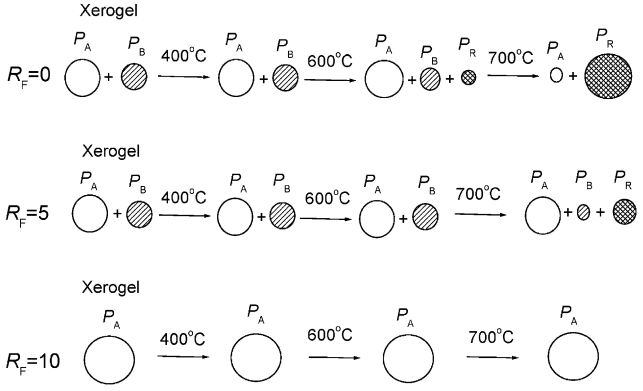

Fig. 4. Schematic model of the phase transformations in the samples calcined at different temperatures. P_A: anatase; P_B: brookite; P_R: rutile. The contents of different phases are roughly illustrated by the area size of the circles.

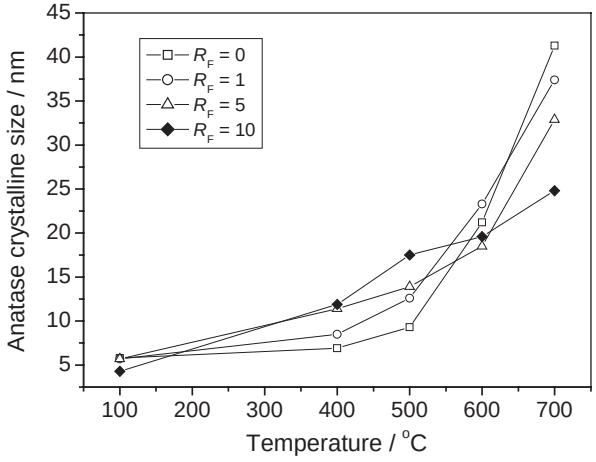

Fig. 5. Effects of calcination temperature and R_F on anatase average crystalline size of TiO_2 powders.

Fig. 5 shows the average crystalline size of anatase in TiO_2 samples as a function of calcination temperature and R_F. At 400°C and 500°C, with increasing R_F, the average crystalline size of anatase increases. This is due to the fact that F^- ions enhance the crystallization of anatase phase, which results in the growth of anatase crystallites [24]. In contrast, at 700°C, with increasing R_F, the average crystalline size of anatase decreases. This is attributed to the fact that the phase transitions accelerate the process of grain growth by providing the

heat of phase transformation ($R_F \leqslant 5$) [31–33], while F^- ions retard the anatase to rutile phase transformation ($R_F \geqslant 10$). Table 1 shows the effect of calcination temperature and R_F on the phase content of TiO_2 [24]. In the temperature range lower than 500°C ($R_F = 0$ or 1) or 600°C ($R_F = 5$), the brookite content slightly decreases with increasing calcination temperature. As there is a corresponding increase in the anatase content, it can be concluded that brookite is gradually converted to anatase over this temperature range. At 700°C ($R_F = 0$ or 1), the brookite disappears. The rutile is dominant and there is only a trace of anatase. It can also be seen from Table 1 that, below 500°C, with increasing R_F, the content of anatase phase increases. This is because the crystallinity of anatase is improved upon F-doping [24,34–36]. It is interesting to note that at temperature below 600°C, the brookite composition decreases with increasing R_F. This phase disappears completely at $R_F \geqslant 10$. A similar trend can also be observed for the rutile phase. At 700°C, the rutile composition decreases with increasing R_F, and it is completely gone at $R_F \geqslant 10$. Therefore, we believe that the F^- ions not only suppress the formation of brookite at low temperature, but also prevent phase transition of anatase to rutile at high temperature.

Table 1
Effects of calcination temperature and R_F on phase content (%) of TiO_2 [24]

R_F	100°C, 8 h	400°C, 1 h	500°C, 1 h	600°C, 1 h	700°C, 1 h
0	A: 64.7 B: 35.3	A: 65.3 B: 34.7	A: 73.5 B: 26.5	A: 79.1 B: 14.0 R: 6.9	A: 5.6 R: 94.4
1	A: 66.9 B: 33.1	A: 69.9 B: 30.1	A: 75.8 B: 24.2	A: 72.0 B: 22.3 R: 5.7	A: 7.8 R: 92.2
5	A: 71.5 B: 28.5	A: 73.5 B: 26.5	A: 76.1 B: 23.9	A: 78.1 B: 21.9	A: 74.5 B: 9.0 R: 16.5
10	A: 100	A: 100	A: 100	A: 100	A: 100
20	A: 100	A: 100	A: 100	A: 100	A: 100

A, B and R denote anatase, brookite and rutile, respectively.

Fig. 6 shows TEM photographs of TiO_2 powders prepared by hydrolysis of TTIP in the H_2O–NH_4F mixed solution with $R_F = 0$ and calcined at (a) 1003°C, (b) 500°C and (c) 700°C. At 100°C, the size of the primary particle is very small and about 5 ± 1 nm. At 500°C, the size of the primary particle increases and is about 12 ± 2 nm, which is in agreement with the value determined by XRD (12.6 nm). At 700°C, some of

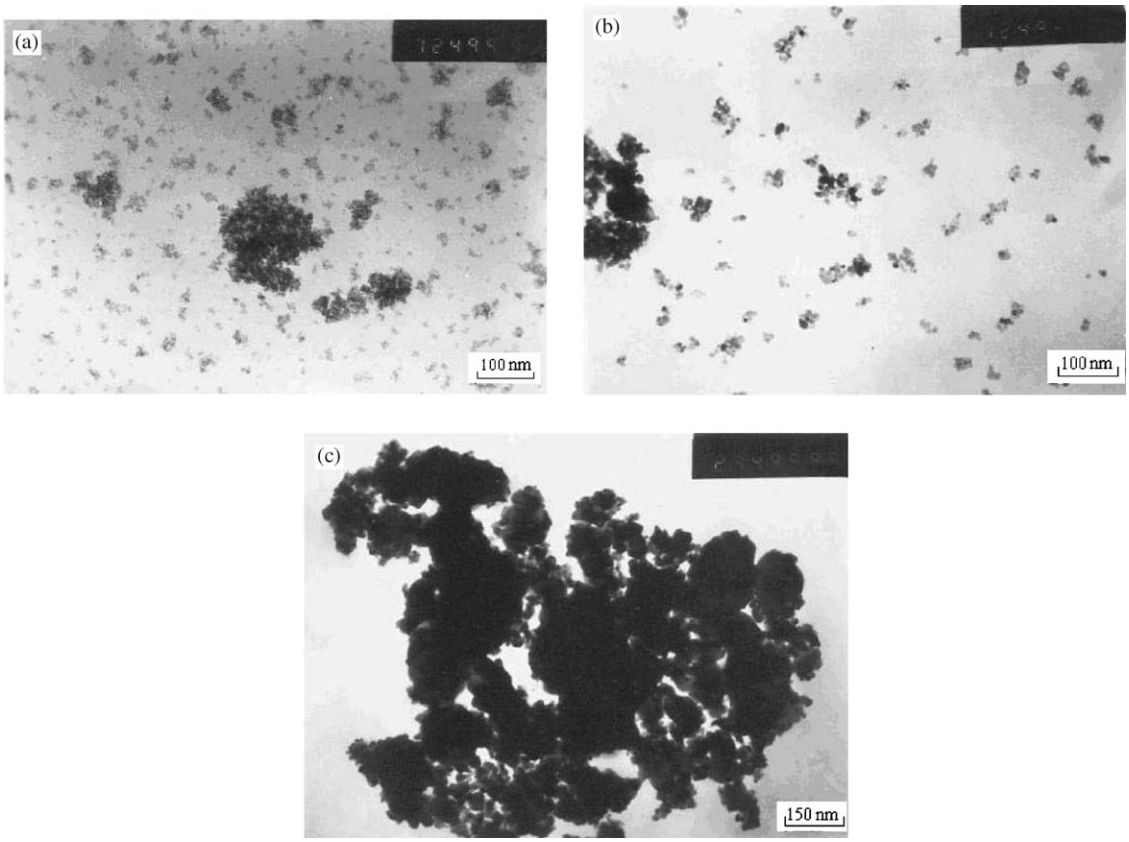

Fig. 6. TEM photographs of TiO_2 powders prepared by hydrolysis of TTIP in the H_2O–NH_4F mixed solution with $R_F = 0$ and calcined at (a) 100°C, (b) 500°C and (c) 700°C.

particles are fused together through sintering, which explains the significant decrease in S_{BET} and disappearance of intra-particle pore structures.

3.2. BET surface areas and pore structure

Fig. 7 shows effects of calcination temperature and R_F on BET specific surface area of TiO_2 powders. At 100°C, all the samples show very large S_{BET} values from 260 to 310 m^2/g. However, the S_{BET} values decrease with increasing calcination temperature due to crystallite growth and sintering. At 700°C, the S_{BET} values of the samples decrease to below 36 m^2/g. Fig. 7 also shows that at 400°C and 500°C, with increasing R_F, the S_{BET} value of TiO_2 powders decreases steadily. On the other hand, at 700°C, with increasing R_F, the S_{BET} value of TiO_2 powders increases. The former may be ascribed to the fact that the more the amount of F^- ions in the TiO_2 xerogels, the stronger the promoting action of TiO_2 anatase crystallization, which would favor the formation of larger TiO_2 crystallites. The latter is due to the fact that the higher the content of F^- ions, the stronger the retarding effects of the anatase on the rutile phase transformation.

Fig. 8 shows the isotherms of pure and doped titania powders at 500°C. All titania powders show isotherms of type IV (BDDT classification) which exhibit hysteresis loops mostly of type H3 [37]. This indicates that the powders contain mesopores (2–50 nm) with narrow slit-like shapes. Also the isotherms of pure TiO_2 powders show two hysteresis loops, showing bimodal pore size distributions in the mesoporous region, as shown in Fig. 9 as calculated from Fig. 8 by BJH method. Bimodal pore size distributions consist of smaller fine (4–10 nm) intra-particle pores and larger (20–120 nm) inter-particle pores. Kumar et al. [38] also reported a bimodal pore size distribution made from fine intra-aggregated pores (represented by the hysteresis loop in the lower P/P_0 range) and larger inter-aggregated pores (hysteresis loop in the higher P/P_0 range) arising from hard aggregates. On the other hand, when $R_F = 20$, the isotherm of F^--doped TiO_2 powders is of type IV with one hysteresis loop of type H3, indicating a monomodal pore size distribution at this temperature arising from the soft aggregates of F^--doped TiO_2 powders at 500°C. Fig. 10 shows SEM photographs of TiO_2 powders prepared from the H_2O–NH_4F mixed solution with $R_F = 0$ (pure water) (a), 5 (b) and 20 (c) and calcined at 500°C for 1 h. Usually, the pores within the hard aggregates give the intra-particle pores, while the voids between these aggregates give the inter-particle pores [14]. It is interesting to observe that with increasing R_F, the particle size of aggregates decreases, which results in inter-particle pores becoming weaker, and finally almost disappearance ($R_F = 20$), as shown in Fig. 9. Fig. 9 also shows that with increasing R_F, the peak pore size of intra-particle pores increases due to the growth of crystallites.

Figs. 11(a) and (b) show the pore size distribution of pure and doped titania powders as a function of calcination temperature. With increasing calcination temperature ($\leqslant$600°C), the peak pore size of the intra-particle pores shifts to the right indicating the growth of pores, while the inter-particle pores almost stay at the same size range and pore volumes. It is also interesting to note that with increasing R_F, the peak pore size of the intra-particle pores shifts to the right indicating the increase of intra-particle pore size due to the growth of anatase crystallite (as shown in Fig. 5). It can be seen from Fig. 11(c) that when $R_F = 20$, at 100°C, the powders exhibit bimodal pore size distributions. However, above 100°C, the powders exhibit monomodal pore size distributions. The pore size distributions of the

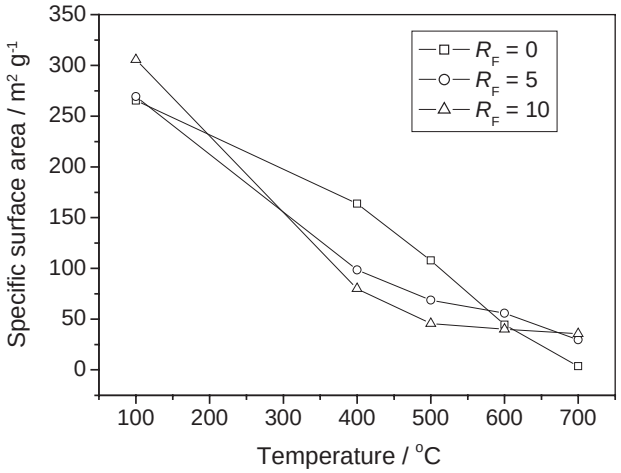

Fig. 7. Effects of calcination temperature and R_F on specific surface area of TiO_2 powders.

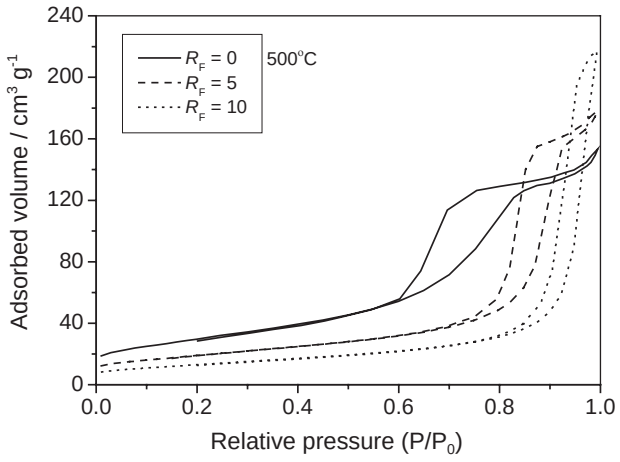

Fig. 8. Isotherms of pure and F-doped TiO_2 powders after being calcined at 500°C for 1 h.

intra-particle pores and inter-particle pores are probably overlapping. This may be ascribed to the fact that the aggregates of powders prepared at $R_F = 20$ are soft aggregates, which results in them becoming weaker or in the disappearance of the inter-particle pores. Moreover, the grain size becomes larger, which results in the size of intra-particle pores shifting to a larger mesoporous region. After being calcined at 700°C, the intra-particle pores of the pure and doped TiO_2 powders disappeared completely as shown in Figs. 11(a) and (b). All the powders exhibit monomodal pore size distributions due to the complete collapse of the intra-particle pores. However, the pore size distribution of inter-particle pores is almost unchanged.

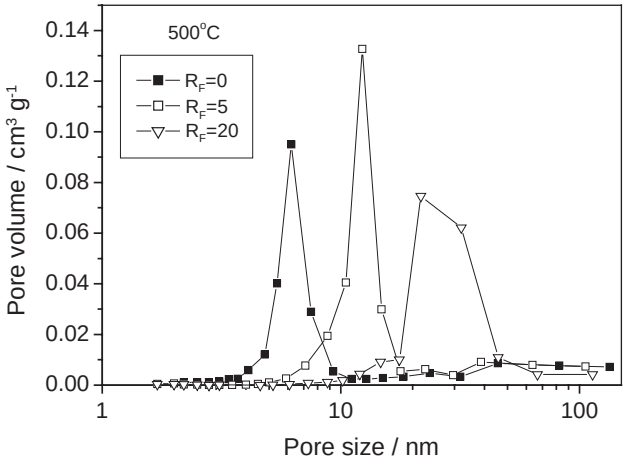

Fig. 9. Pore size distributions of pure and F-doped TiO_2 powders after being calcined at 500°C for 1 h.

Another interesting result from Fig. 11 is that the main cause of the disappearance of most intra-particle pores at 700°C could be attributed to grain growth from the phase transformation of anatase to rutile, as confirmed in Figs. 4 and 6. Kumar et al. [27] also investigated the microstructures of titania membranes calcined at various temperatures by high resolution scanning electron micrograph. They found that the powders before the anatase to rutile transformation contain small anatase crystallites, but the powders after phase transformation have smaller anatase crystallites and bigger densified rutile regions. It is thought that smaller anatase crystallites grow into bigger rutile crystallites through the transformation, leading to the disappearance of the voids among anatase crystallites which results in the collapse of intra-particle pores in the bimodal pore size distributions.

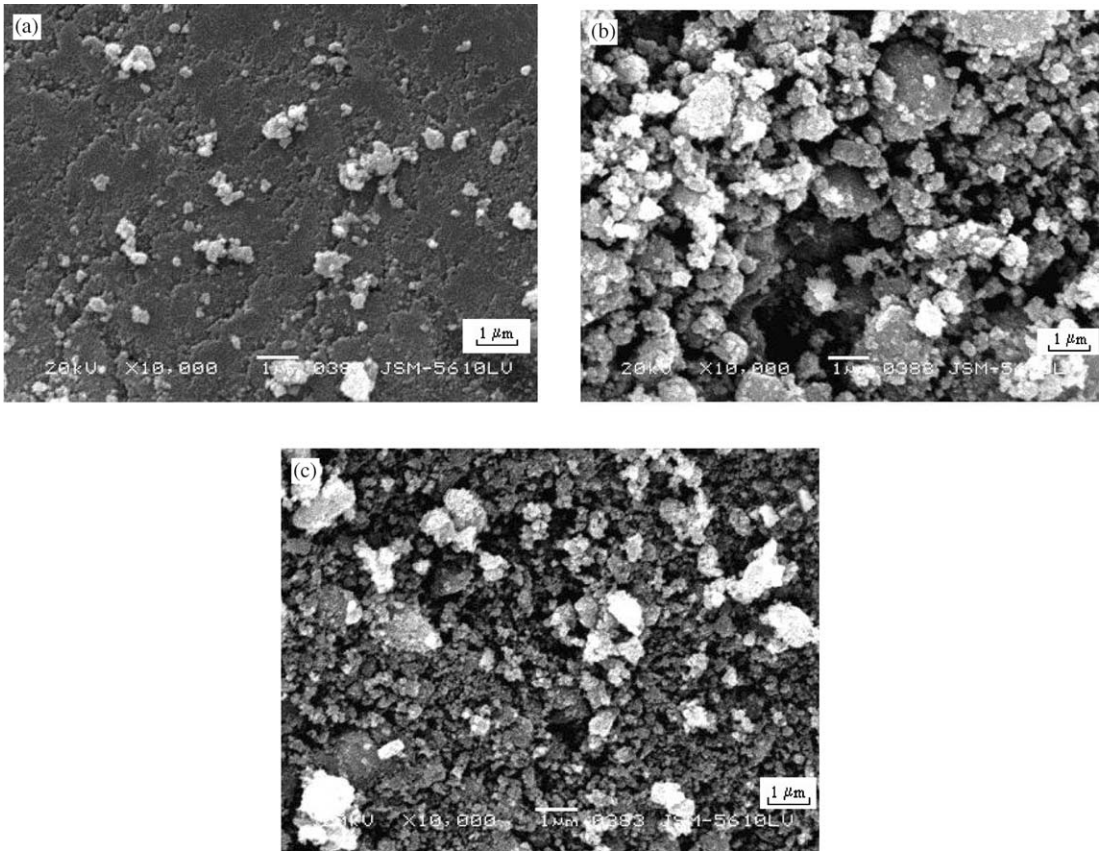

Fig. 10. SEM photographs of TiO_2 powders prepared from the H_2O–NH_4F mixed solution with $R_F = 0$ (pure water) (a), 5 (b) and 20 (c) and dried at 500°C for 1 h.

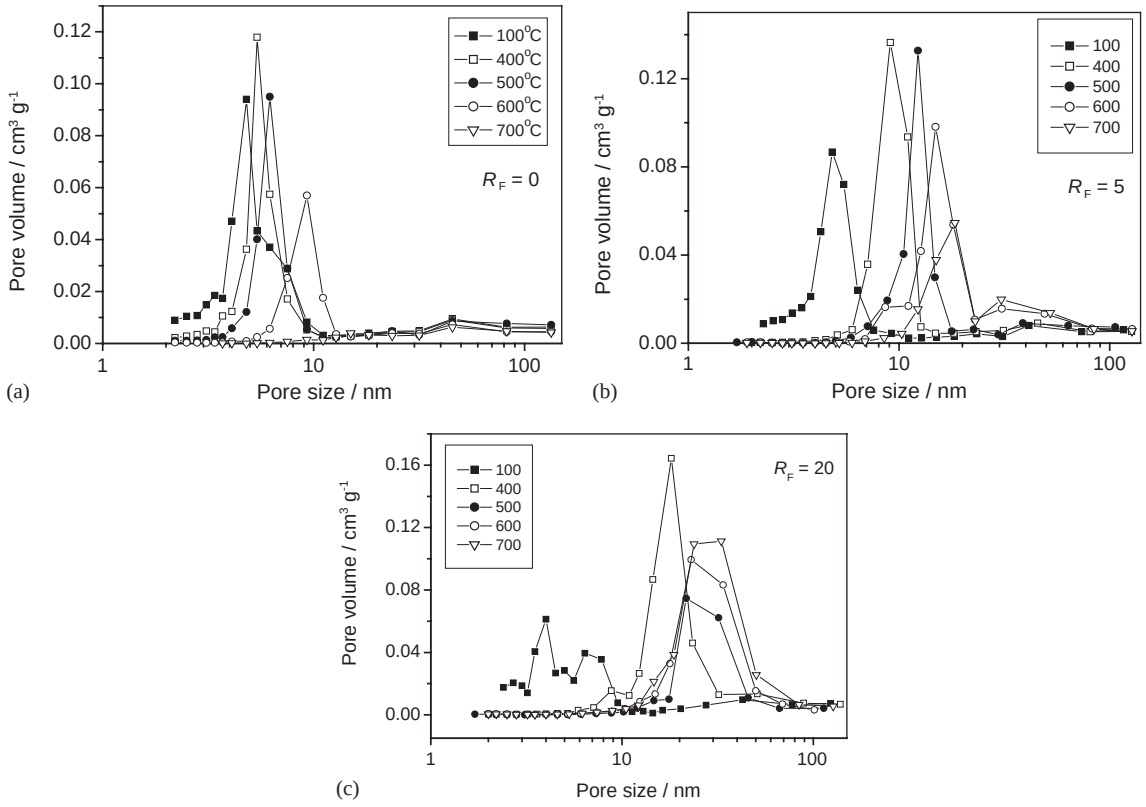

Fig. 11. Evolution of pore size distributions as a function of temperatures: (a) $R_F = 0$, (b) $R_F = 5$ and (c) $R_F = 20$.

The effects of F^--doping and calcination temperature on textural evolution of mesoporous TiO_2 powders were investigated by TEM, SEM and N_2 adsorption method. The results shows that with increasing R_F, the peak pore size of the intra-particle pores increases due to the enhancement in anatase crystallization (as shown in Fig. 5). When $R_F = 20$, at 100°C, the powders exhibit bimodal pore size distributions. However, above 100°C, the powders exhibit monomodal pore size distributions due to the soft aggregates of F^--doped TiO_2 powders.

4. Conclusions

1. The crystallization of anatase was obviously enhanced due to F^--doping at 400°C and 500°C. Moreover, with increasing F^- ion concent, F^- ions not only suppressed the formation of brookite phase at low temperature, but also prevented phase transition of anatase to rutile at high temperature.
2. The BET surface area of all the powders dried at 100°C ranged from 260 to 310 m^2/g as determined by nitrogen adsorption. With increasing calcination temperatures, the S_{BET} values of the calcined titania powders decreased due to the increase in crystalline size.
3. The pore size distribution was bimodal with fine intra-particle pore and larger inter-particle pore as determined by nitrogen adsorption isotherms. The peak pore diameter of intra-particle pore increases with increasing F^- ion content. At 700°C, all the titania powders exhibit monomodal pore size distributions due to the complete collapse of the intra-particle pores.
4. With increasing R_F, the peak pore size of the intra-particle pores increases. When $R_F = 20$, at 100°C, the powders exhibit bimodal pore size distributions. However, above 100°C, the powders exhibit monomodal pore size distributions probably due to the overlapping of the size of intra-particle pores and inter-particle pores.

Acknowledgments

This work was partially supported by the National Natural Science Foundation of China (50272049), The Excellent Young Teachers Program of MOE of PRC, and the Project-Sponsored by SRF for ROCS of SEM. This work was also financially supported by a grant from the National Natural Science Foundation of China and Research Grant Council of the Hong Kong Special

Administrative Region, China (Project No. N_CUHK433/00).

References

[1] K. Honda, A. Fujishima, Nature 238 (1972) 37–38.
[2] M.R. Hoffmann, S.T. Martin, W. Choi, D.W. Bahnemann, Chem. Rev. 95 (1995) 69–96.
[3] A. Fujishima, T.N. Rao, D.A. Tryk, J. Photochem. Photobiol. C: Photochem. Rev. 1 (2000) 1–23.
[4] B. O'Regan, M. Graetzel, Nature 353 (1991) 737–739.
[5] K.N.P. Kumar, K. Keizer, A.J. Burggraaf, T. Okubo, H. Nagamoto, S. Morooka, Nature 358 (1992) 48–51.
[6] K.C. Song, S.E. Pratsinis, J. Mater. Res. 15 (2000) 2322–2329.
[7] K.C. Song, S.E. Pratsinis, J. Colloid Interface Sci. 231 (2000) 289–298.
[8] K.C. Song, S.E. Pratsinis, J. Am. Ceram. Soc. 84 (2001) 92–98.
[9] G.W. Koebrugge, L. Winnubst, A.J. Burggraaf, J. Mater. Chem. 3 (1993) 1095–1112.
[10] C.J. Brinker, G.W. Scherer, Sol–Gel Science Academic Press, San Diego, CA, 1990, p. 518.
[11] C.J. Brinker, R. Sehgal, S.L. Hietala, R. Deshpande, D.M. Smith, D. Loy, C.S. Ashley, J. Membr. Sci. 94 (1994) 85–93.
[12] H.K. Bowen, Mater. Sci. Eng. 65 (1986) 1574–1582.
[13] C.H. Chang, R. Gopalan, Y.S.A. Lin, J. Membr. Sci. 91 (1994) 27–45.
[14] J. Kim, K.C. Song, S. Foncillas, S.E. Pratsinis, J. Eur. Ceram. Soc. 21 (2001) 2863–2872.
[15] K.N.P. Kumar, K. Keizer, A.J. Burggraaf, J. Mater. Chem. 3 (1993) 917–922.
[16] J. Yang, Y.X. Huang, J.M.F. Ferreira, J. Mater. Sci. Lett. 16 (1997) 1933–1935.
[17] J. Yang, J.M.F. Ferreira, Mater. Lett. 36 (1998) 320–324.
[18] J. Yang, J.M.F. Ferreira, Mater. Res. Bull. 33 (1998) 389–394.
[19] S. Vargas, R. Arroyo, E. Haro, R. Rodriguez, J. Mater. Res. 14 (1999) 3932–3937.
[20] K. Yanagisawa, J. Ovenstone, J. Phys. Chem. B 103 (1999) 7781–7787.
[21] H. Yin, Y. Wada, T. Kitamura, S. Kambe, S. Murasawa, H. Mori, T. Sakata, S. Yanagida, J. Mater. Chem. 11 (2001) 1694–1703.
[22] J.G. Yu, J.C. Yu, B. Cheng, X.J. Zhao, J. Sol–Gel Sci. Tech. 24 (2002) 39–48.
[23] J.G. Yu, J.C. Yu, X.J. Zhao, J. Sol–Gel Sci. Tech. 24 (2002) 95–103.
[24] J.C. Yu, J.G. Yu, W.K. Ho, Z.T. Jiang, L.Z. Zhang, Chem. Mater. 14 (2002) 3808–3816.
[25] J.C. Yu, J.G. Yu, L.Z. Zhang, W.K. Ho, J. Photochem. Photobio. A: Chem. 148 (2002) 263–271.
[26] H. Zhang, J.F. Banfield, J. Phys. Chem. B 104 (2000) 3481–3487.
[27] K.N.P. Kumar, K. Keizer, A.J. burggraaf, J. Mater. Chem. 3 (1993) 1141–1149.
[28] Y.S. Lin, C.H. Chang, R. Gopalan, Ind. Eng. Chem. Res. 33 (1994) 860–865.
[29] H.Z. Zhang, M. Finnegan, J.F. Banfield, Nano Lett. 1 (2001) 81–84.
[30] E.P. Barrett, L.G. Joyner, P.H. Halenda, J. Am. Chem. Soc. 73 (1951) 373–381.
[31] J.C. Yu, J.G. Yu, W.K. Ho, L.Z. Zhang, Chem. Commun. (2001) 1942–1943.
[32] X. Ye, J. Sha, Z. Jiao, L. Zhang, Nanostruct. Mater. 7 (1997) 919–921.
[33] J.G. Yu, J.C. Yu, W.K. Ho, Z.T. Jiang, New J. Chem. 26 (2002) 607–613.
[34] A. Hattori, M. Yamamoto, H. Tada, S. Ito, Chem. Lett. (1998) 707–708.
[35] A. Hattori, K. Shimoda, H. Tada, S. Ito, Langmuir 15 (1999) 5422–5426.
[36] A. Hattori, H. Tada, J. Sol–Gel Sci. Tech. 22 (2001) 47–51.
[37] K.S.W. Sing, D.H. Everett, R.A.W. Haul, L. Moscou, R.A. Pierotti, J. Rouquerol, T. Siemieniewska, Pure Appl. Chem. 57 (1985) 603–619.
[38] K.N.P. Kumar, J. Kumar, K. Keizer, J. Am. Ceram. Soc. 77 (1994) 1396–1400.